Invited Paper

Generation of High Power THz Waves in Relativistic Electron Beam Plasma and Two-Sheet-Beam FEM

M.K.A. Thumm [1*, 5*], A. V. Arzhannikov [1, 2], V.T. Astrelin [1, 2], A.V. Burdakov [1-3], N.S. Ginzburg [4], I.A. Ivanov [1, 2], P.V. Kalinin [1, 2], S. A. Kuznetsov [1, 2], M.A. Makarov [2], K. I. Mekler [2], A.G. Paulish [1], N. Yu. Peskov [4], S. V. Polosatkin [1, 2], S.A. Popov [2], V. V. Postupaev [1, 2], A. F. Rovenskikh [2], A.S. Sergeev [4], S. L. Sinitsky [1, 2], V. F. Sklyarov [2, 3], V.D. Stepanov [1, 2], L. N. Vyacheslavov [1, 2], V. Yu. Zaslavsky [4]

[1] Novosibirsk State University (NSU), Novosibirsk, Russia

[*1] Email: thumm@nsm.nsu.ru

[2] Budker Institute of Nuclear Physics (BINP) SB RAS, Novosibirsk, Russia

[3] Novosibirsk State Technical University (NSTU), Novosibirsk, Russia

[4] Institute of Applied Physics (IAP) RAS, Nizhny Novgorod, Russia

[5] Karlsruhe Institute of Technology (KIT), IHM, Karlsruhe, Germany

[*5] Email: manfred.thumm@kit.edu

(Received December 23, 2011)

Abstract: Sub-mm wave and THz radiation can be generated by the process of transformation of plasma waves into electromagnetic (EM) radiation at strong Langmuir (LT) turbulence via a two-stream instability induced by a propagating high current relativistic electron beam (REB). Plasmon scattering on plasma density fluctuations yields EM emission at the plasma frequency ω_p ("ω_p-process"). Nonlinear plasmon-plasmon merging results in the generation of photons nearby the 2nd harmonic of the plasma frequency $2\omega_p$ ("$2\omega_p$-process"). For plasma densities 10^{14}–10^{15} cm^{-3}, corresponding radiation frequencies are located in the range of sub-mm waves: 180-566 *GHz*. The power density of LT-induced sub-mm-wave emission from plasmas in the multi-mirror trap GOL-3 (BINP) during injection of a 10-μs-REB at plasma densities $n_e \approx 5 \cdot 10^{14}$ cm^{-3} , electron temperatures $T_e \approx 1.5$ *keV* and magnetic field $B \approx 4$ *T* was measured to be up to 5-10 kW/cm^3 in the frequency band above 100 *GHz*.

Former experiments on the ELMI device (BINP) demonstrated the operation of an mm-wave single channel free electron maser (FEM) with planar cavity geometry and 2D distributed feedback. Measurements have shown single mode single-frequency generation (75 *GHz*) with about 300 ns pulse duration at the power level of 20-40 *MW*. In the case of two parallel sheet electron beams in two slit channels, we plan to investigate an inter-cavity scattering scheme for two-stage generation of sub-mm wave radiation. As a first step we have studied simultaneous generation and transport of two intense sheet electron beams in two FEM slit channels. The REB parameters were the following: electron energy 0.8 *MeV*, total current of each beam 3 *kA*, cross section 0.4 *cm* x 7 *cm* and pulse duration 3 μs. The measurements of the energy of the mm-wave radiation pulse for frequencies higher than 70 *GHz* gave a value of 4-6 *J* and the average power of 20-40 *MW* from each of the two FEM channels.

Both the GOL-3 and FEM experiments need components and systems for spectral diagnostics of sub-mm wave radiation. Novel micro-structured quasi-optical elements have been developed where amplitude, phase and polarization responses are controlled by frequency selective surface (FSS) topologies, manufactured by photolithography and electroforming. Bandpass filters (70 *mm* aperture diameter) with center frequency (CF) from 112 to 376 *GHz* show > 90% transmission and have a FWHM bandwidth of ~ 12%. Meta-material absorbers for real-time THz imaging (CF from 310 to 370 *GHz*) have an absorption of > 90% and excellent thermal insulation.

Keywords: Terahertz generation and spectroscopy, Electron beam plasma, Free electron maser, Frequency selective surfaces

doi: 10.11906/TST.018-039.2012.03.03

1. Introduction and background

One of possible ways to generate sub-millimeter and THz radiation is to use the process of transformation of plasma waves into electromagnetic (EM) radiation at strong Langmuir turbulence [1-3]. Such conditions can exist either in space plasmas [4-5] or in a laboratory plasma heated by a high-power particle beam [6]. First sub-THz emission studies on the multi-mirror machine GOL-3 at BINP Novosibirsk were reported in [7-8]. The mechanism of plasma heating was recognized as the excitation of strong Langmuir turbulence (LT) via a two-stream instability induced by the propagating high current relativistic electron beam (REB). The detailed theoretical consideration of LT-induced EM distinguishes two main processes. First, plasmon scattering on plasma density fluctuations yields EM emission at the plasma frequency ω_p ("ω_p-process"). Second, non-linear plasmon-plasmon merging results in production of photons in the vicinity of the double plasma frequency $2\omega_p$ ("$2\omega_p$-process"). For plasma densities between 10^{14}-10^{15} cm^{-3}, the corresponding output radiation frequencies are located in the range from mm- to sub-mm-waves, f_p = 90-283 *GHz* and $2f_p$ = 180-566 *GHz*. In this paper, we present studies of sub-THz emission from GOL-3 plasmas during injection of a 10-μs-REB. We intentionally focused on investigating the $2\omega_p$-emission from the plasma at plasma density $n \approx 10^{14}$–10^{15} cm^{-3}, and magnetic field strength of 4 *T*.

In experiments on the ELMI-device at BINP Novosibirsk, the operation of a 4-*mm* single channel free electron maser (FEM) with planar geometry and two-dimensional distributed feedback had been demonstrated [9]. In this regime the measurements of the spectral and spatial properties of the generated EM radiation using heterodyne diagnostics at the output of the FEM had shown single-mode and single-frequency operation around 75 *GHz* with a pulse duration of about 300 *ns* at the power level of 20-40 *MW*. These results provide a basis for the development of a multichannel planar 75 *GHz* FEM with a factor of ten larger output power by using 2-D distributed feedback. For the case of two parallel sheet beams in two slit channels, it was proposed to exploit an inter-cavity scattering scheme for two-stage generation of sub-mm wave radiation (0.6 *THz*) [10]. As the first step of experimental realization of this idea we have studied simultaneous generation and transport of two intense sheet electron beams in two parallel slit channels [11], which are similar to the electrodynamic system of the proposed two-channel sub-mm wave FEM. In these experiments the parameters of the generated REBs were the following: 0.8 *MeV* electron energy, 3 *kA* total current of each beam, 0.4 *cm* x 7 *cm* cross section and 3 μs pulse duration. Electron-optical experiments demonstrated that these REBs can be successfully transported in two parallel slit vacuum channels with a cross section of 0.95 *cm* x 9 *cm* and a length of 1.3 *m* in a guiding magnetic field of up to 1.7 *T*.

Both the GOL-3 multi-mirror trap plasma and ELMI-FEM experiments require the development of components and systems for spectral diagnostics of sub-mm wave and THz radiation. The basis for these novel devices are micro-structured quasi-optical elements where amplitude, phase and polarization responses are controlled by frequency selective surface (FSS) topologies, manufactured by photolithography and electroforming. The present paper reports about electromagnetic modeling and optimization, design and fabrication, and device testing and calibration of narrow band pass filters with high transmission and diameters up to 70 *mm* and of meta-material absorbers for real-time 2D THz imaging. These 2D sub-mm wave matrix receivers are inexpensive, easy-to-use, fast-response, sensitive, high-resolved, large-formatted, and can be operated at room temperature.

2.Generation of sub-THz radiation in turbulent plasmas by plasmon-plasmon merging

2.1. Experimental setup and background physics

Experimental studies have been carried out at the multiple-mirror magnetic trap GOL-3 at BINP (Fig. 1). The main objectives of its research program are the physics of collective plasma heating by a high-power REB and the physics of plasma confinement in a multi-mirror (periodically modulated along the axis) magnetic field (see, e.g., [12-13]). The major parameters and operational regimes of GOL-3 are: deuterium plasmas are confined in a 12-meter-long solenoid, which has 52 corrugation periods (cells of multimirror system) of 22 *cm* length each; the magnetic field in the maxima is 4.8 *T* and that in the minima 3.2 *T*. The mirror ratio of the corrugated field is 1.5. The solenoid ends are provided by magnetic mirrors with a field of 8-9 *T*. In the experiments being discussed here, the deuterium plasma had a density of $(1\div8)\times10^{14}$ cm^{-3} with a bell-shaped axial density profile (due to gas-puffing technology where some dense gas was also puffed into the beam compression area). Plasma heating is provided by the high-power REB. The electron beam is initially generated in a sheet (planar) diode of the U-2 accelerator. After compression by a magnetic field it gets circular cross-section. Then this REB is injected through one end and propagates in the plasma along the magnetic field lines. The main parameters of the REB are: energy ~ 0.7 *MeV*, current ~ 20 *kA*, pulse duration ~ 12 μs, and initial energy content ~ 90 *kJ*.

The plasma in the GOL-3 is initially created by a high-current linear discharge along the magnetic field. The cold plasma diameter is ~8 *cm* and the electron beam diameter at B = 3.2 *T* is approximately 4 *cm*. When the REB is injected into the plasma, a strong collective relaxation of the beam electrons is observed. The classical free path length of a single beam electron in the GOL-3 plasma is some thousand *km*, nevertheless we observe a strong average deceleration of the beam electrons. The measured mean energy loss of the beam electrons can exceed 50% after passing the plasma column [14]. The plasma heating is highly non-uniform along the axis. That was naturally explained by the concurrence of several processes, including gradual degradation of the REB quality, change of the ratio of electron beam density to plasma density, particle and energy transport, etc. A typical experimental scenario is shown in Fig. 2 and almost linear growth of the plasma pressure is shown in Fig. 3.

In this paper we will mainly concentrate on the first phase of the experiment when the high-power REB is injected into the plasma. In this phase a high-level Langmuir turbulence is pumped during the beam-plasma interaction. The turbulence in turn dramatically affects the properties of the plasma. Following ref. [13] we will briefly summarize the known collective phenomena in the GOL-3 plasma.

- Turbulent Langmuir waves of high amplitude are excited by the REB in the plasma when the increment of the two-stream instability exceeds the electron collision rate, therefore high beam current density and good beam quality are required;
- Effective heating of plasma electrons occurs in the turbulent fields with main fraction of the energy lost by the electron beam being transferred to a high-energy tails of electron distribution;
- The high-energy electron tails escape from the turbulent plasma in the trap at near the time-of-flight rate, so in the peak of heating the plasma contains up to ~5% of the initial beam

energy despite the fact that a much higher fraction of energy was lost by the beam electrons;

- At the same time axial electron thermal conductivity is suppressed by ~3 orders of magnitude due to the turbulence [15-16];
- Due to the non-uniformity of heating and suppression of the heat transport strong gradients of electron pressure arise in the corrugated magnetic field during the beam pulse [17];

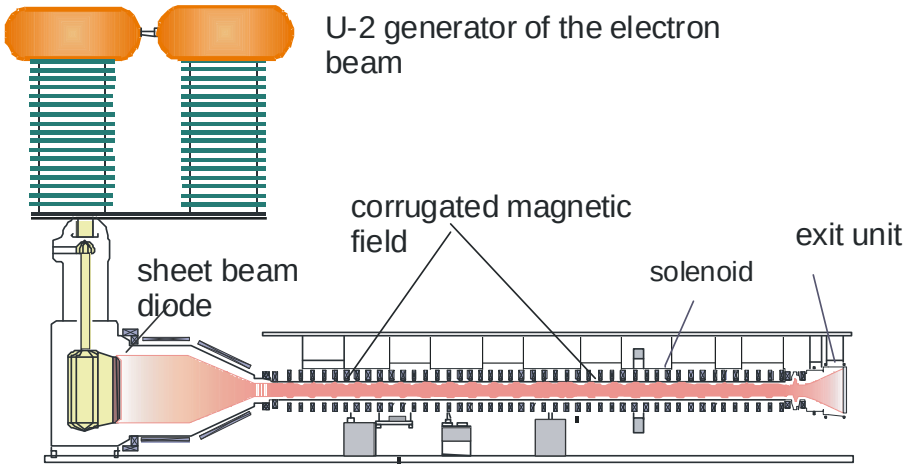

Fig.1 Schematic of the GOL-3 multi-mirror magnetic trap.

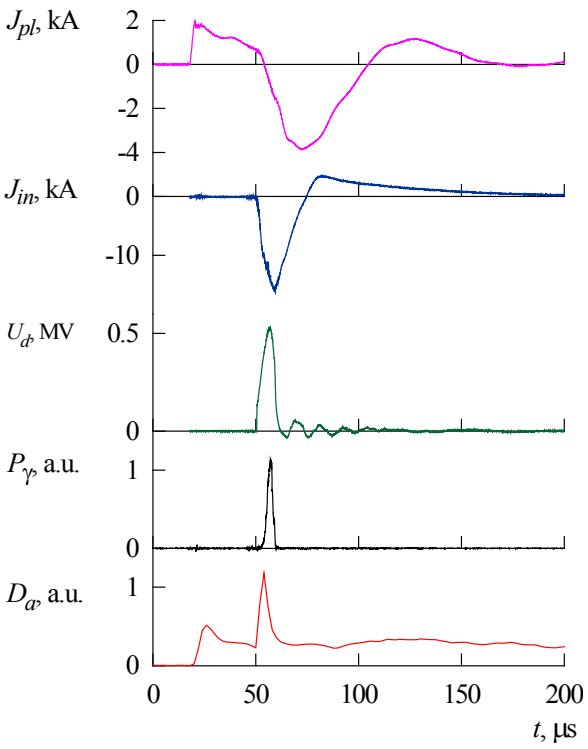

Fig. 2 GOL-3 experimental scenario. The following waveforms are shown: current of the pre-ionization discharge J_{pl}, input REB current J_{in}, diode voltage U_d, hard bremsstrahlung P_γ and brightness of D_α line. The pre-ionization discharge starts at ~15 μs, and the beam injection at ~50 μs.

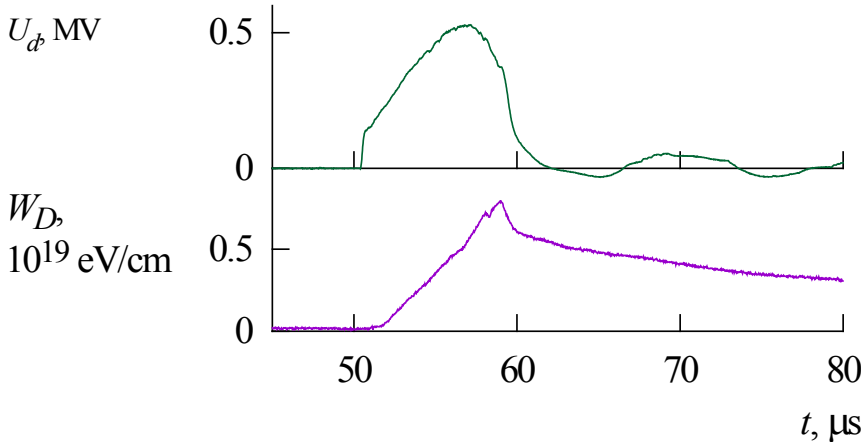

Fig. 3 Dynamics of plasma heating in a typical shot (the same as in the previous Figure). Waveforms of diode voltage U_d and diamagnetic signal W_D are shown at $z = 264$ *cm* from the input mirror.

- Fast collective ion acceleration followed by thermalization occurs together with a total plasma flow along the system due to electron pressure gradients [16-17];
- Interaction between trapped and transit ions in high-pressure-gradient zones excites an ion bounce instability [12], [18] that increases exchange between the two particle groups and suppresses axial plasma flow.

Some other important collective effects that are not directly connected with the microwave generation efficiency are a self-organization of current in the plasma [19] and improvement of energy confinement time over classical predictions at low densities [12]. This listing of collective phenomena shows that the plasma dynamics in the multiple-mirror trap is mainly determined by turbulent processes. Turbulent scattering of electrons increases the effective collision rate. This enhanced collision rate can saturate the two-stream instability which determines the efficiency of REB relaxation in the plasma. In the case of the bounce instability the free mean path length of transit ions decreases and particle exchange between transit and trapped ions occurs more effectively in the end cells of the trap.

Registration of EM emission was performed at two distances from the beam injection plane: about 0.8 *m* and 1.8 *m*, where the magnetic field is $B \cong 4$ *T* (see Fig. 4). Diamagnetic signals show that the maximum efficiency of REB-plasma interaction is in this area. Information about the intensity of the beam-plasma interaction was obtained by comparison of measurements of the electron energy distribution function before injection into the plasma and after passing through the plasma column.

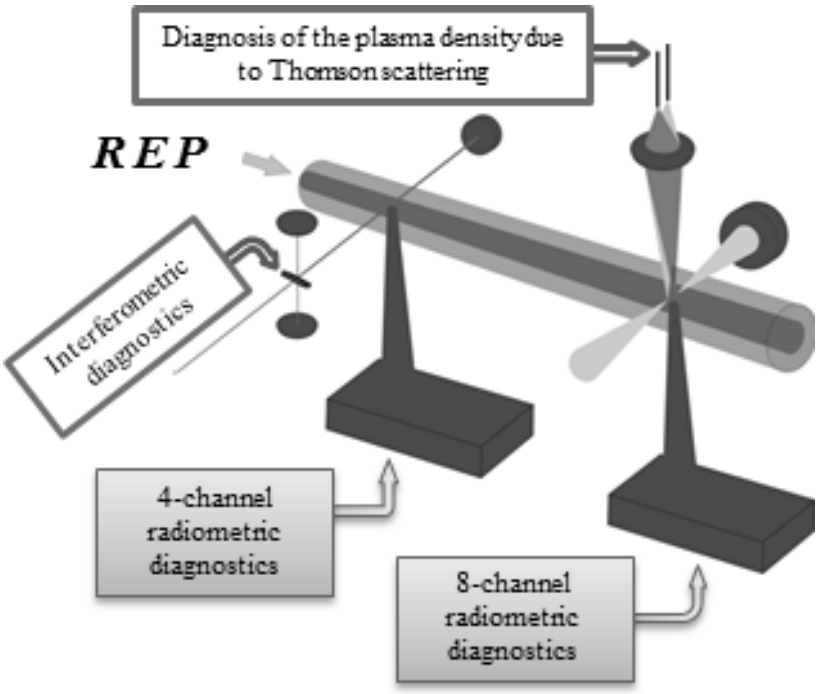

Fig. 4 Schematic of the radiometric experiment at the GOL-3 multi-mirror-trap facility.

Since the frequency spectrum of the sub-THz radiation and its dynamics during the REB injection are essentially dependent on the plasma parameters, we apply a Thomson scattering diagnostic system based on an Nd-glass laser (1.054 μm). The laser generates two independently triggered pulses with 10-20 J energy and 20-40 ns duration each. The time delay between the two pulses can be varied from 0.1-100 μs. This system allows us to measure the plasma density at eight locations over the plasma cross section at a distance of 1.4 m from the REB injection point. In some experiments the Thomson scattering system was also used to measure the velocity distribution function of heated plasma electrons. Time dynamics of the integrated plasma density is registered at a distance of 0.8 m from the REB injection point by a Michelson interferometer based on a CO_2 laser.

We developed two radiometric systems capable of measuring the power of the sub-mm wave emission. One of them has 4 parallel frequency-shifted spectral bands in the interval from 260 GHz up to 400 GHz. The other covers the interval from 110 GHz up to 380 GHz with 8 channels. The filters of this high-resolution system have a relative transition bandwidth of ~12% and an out-of-band attenuation of 50 dB at 20-60 GHz frequency shift of adjacent transmission bands. After passing through the filters, the sub-mm wave beams are focused by aspheric PTFE (Teflon) lenses (f= 40 mm, diameter = 70 mm) into the receiving horn antennas of the Schottky-detector units. Each detector, initially developed for operation at frequencies 210-450 GHz, is equipped with a built-in 900 MHz-band operational preamplifier and has a response time better than 2 ns. At 50 Ω loading resistance, the detector Volt-Watt sensitivities and dynamic ranges, precisely measured with calibrated 280 GHz-solid-state radiation-source, are within 1000-4000 V/W and 50 dB, respectively. The broadband calibration of the detectors with a tunable backward-wave oscillator has shown an acceptable level of their sensitivity up to ~530 GHz. Details of design and operation of the spectrometers are discussed in Chapter 4.

2.2. Experimental results

In our first experiments we confirmed that the spectrum of the emitted EM radiation essentially depends on the plasma density in the investigated area of the plasma column. For example, in the case of constant plasma density of $n_0 \approx 3 \cdot 10^{14}\ cm^{-3}$ during 6 μs of electron beam injection the radiated spectrum is broad and we measured a slowly varying ratio between the signals for three frequency bands [8]: 275*GHz*, 312 *GHz*, and 350 *GHz* with the maximal radiation power at the 312 *GHz*.

The opposite case is when the plasma density increases during the REB injection time. This occurs when the ionization degree of hydrogen at the start of beam injection is about 50% and then it increases up to 100% with the increase of the plasma electron temperature up to 2-3 *keV*. For the final values of the plasma density $n_e \approx 5 \cdot 10^{14}\ cm^{-3}$ and $n_e \approx 7 \cdot 10^{14}\ cm^{-3}$ the dynamics of the emitted radiation in selected frequency bands is plotted in Fig. 5 (shot PL10639 and shot PL10653, respectively). One can see that the increase of the plasma density during the injection time causes some up-shifting of the position of the maximum of the spectral power density. We also measured that the increase of the frequency for the maximal sub-mm wave radiation power is not the only effect but also the spectral interval of the generated radiation is narrowed during the increase of the plasma density.

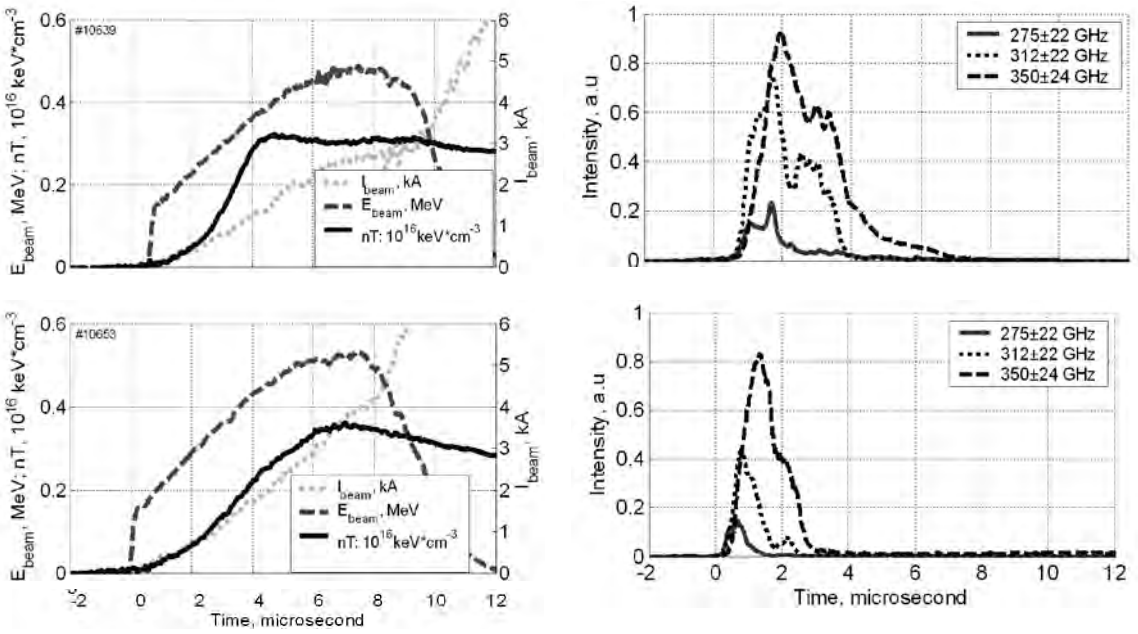

Fig. 5 Two shots at different plasma densities reached during the beam injection:
PL10639 - $n_e \approx 5 \times 10^{14}\ cm^{-3}$, PL10653 - $n_e \approx 7 \times 10^{14}\ cm^{-3}$. The REB current is given in tens of *kA*. The signals of the sub-THz detectors were digitally smoothened in order to make a direct comparison more evident.

Such behavior of the distribution of the EM-radiation power over the frequency channels can be explained by the dependence of the frequency spectrum of the generated EM-radiation on the ratio of electron cyclotron frequency to the plasma frequency. When the ratio decreases, the EM-radiation spectrum has to be more narrow [20]. On the basis of this dependency we hope to achieve in future experiments a smaller width of the generated spectrum by increasing the plasma density and by employing a lower strength of the magnetic field.

At z = 0.8 *m* the power density of LT - induced sub-mm-wave emission during injection of a 10-μs-REB at plasma densities of $n \approx 10^{14}-10^{15}$ cm^{-3} and magnetic $B \approx 4$ T was measured to be up to 5-10 kW/cm^3 in the frequency band above 100 *GHz*. Theoretical estimations [3] assuming a ratio of the energy density of the LT to the total plasma energy density of 0.1 result in a theoretical value of 7 kW/cm^3. The measured maximal power level of $2\omega_p$-emission is localized close to the region with maximal plasma pressure at around 0.8 *m* from the REB injection point (see Fig. 6) and increases with increasing magnetic field due to the increasing plasma pressure (see Fig. 7).

In all experiments we observed sub-THz radiation from the plasma only during the REB injection time. In no case sub-THz power was measured outside this time interval. Actually the end of sub-THz emission occurs even somewhat earlier, when the energy of the beam electrons (which is represented by the cathode voltage U_d) significantly decreases from the maximum. At this moment of time all other plasma properties except that the pumping of the LT by the REB remain practically unchanged, including high average energy of plasma electrons. In a special experiment we have checked also that no EM radiation in the $2\omega_p$-emission frequency band was generated during injection of the electron beam into vacuum. Therefore we can exclude different electron cyclotron mechanisms as possible source of the observed sub-THz radiation.

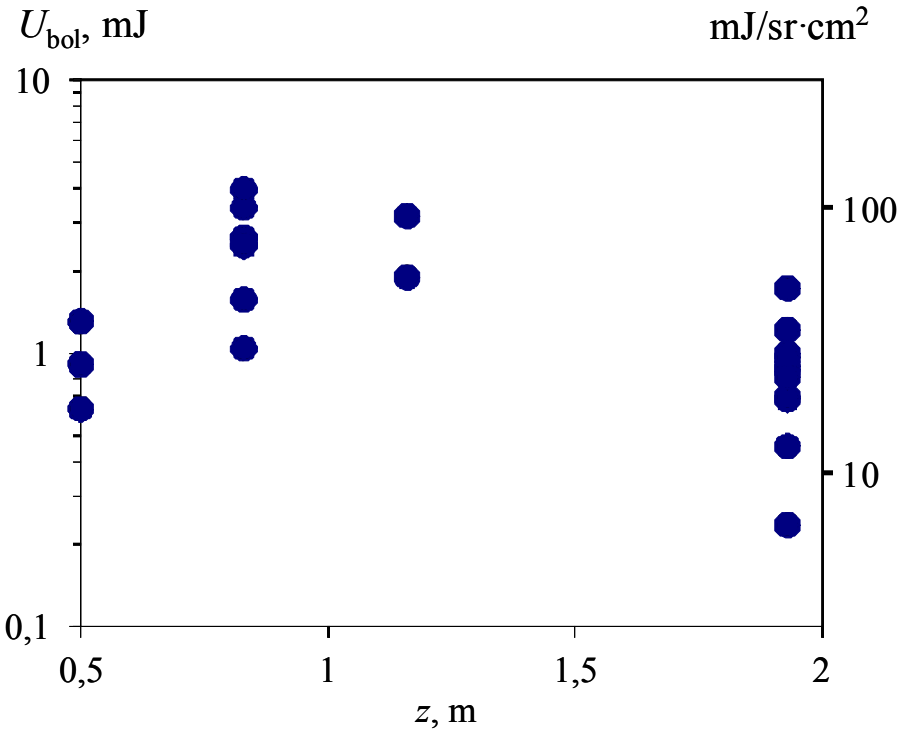

Fig. 6 Total energy of emitted EM radiation measured by the bolometer along the plasma column from z = 0.5 *m* to 2.0 *m*.

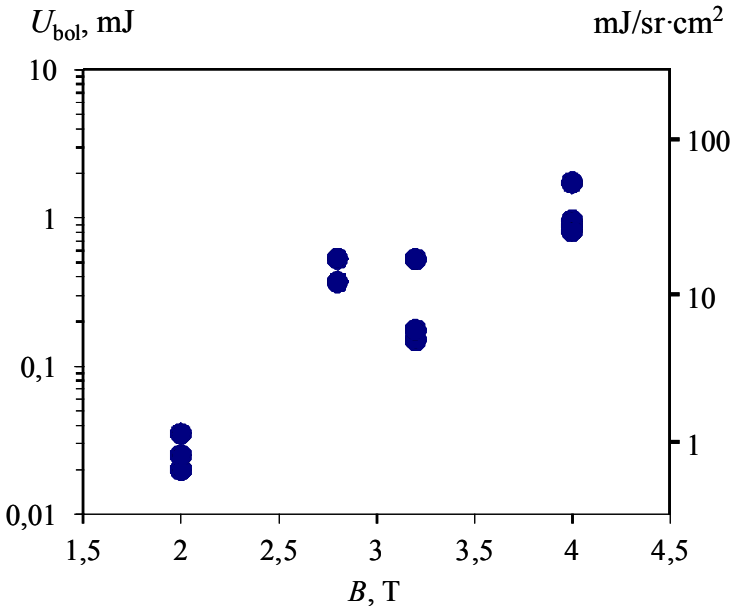

Fig. 7 Total energy of emitted EM radiation in dependence of the magnetic field measured by the bolometer at z = 0.8 *m*.

The next interesting feature of the sub-THz plasma emission in the GOL-3 experiment is its temporal structure. Usually short spikes that last for 2-100 *ns* are observed during the EM emission. Such short spikes might indicate that the generation of sub-THz radiation occurs simultaneously in a large number of compact zones within the plasma. A special experiment [14] with tenfold reduction of the REB cross-section was performed. All other specific electron beam and plasma parameters remained the same as in the full-scale experiments. In that experiment the beam-heated cross-section of the plasma becomes correspondingly smaller with less generation centers. EM emission in this case became highly spiked (see Fig. 8).

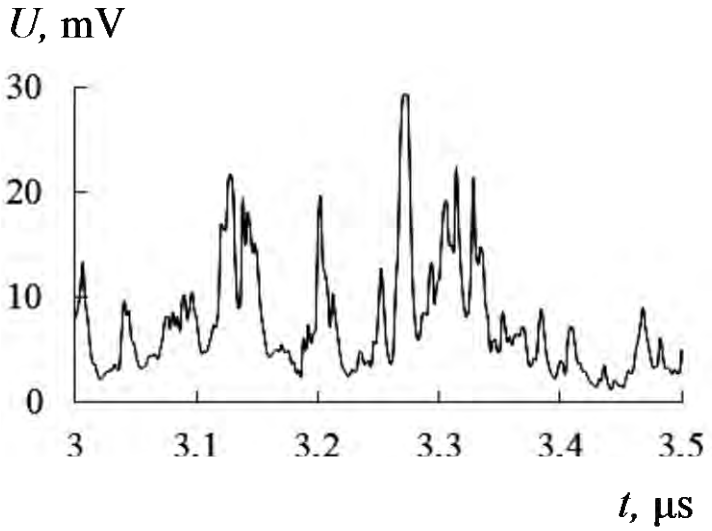

Fig. 8 Temporal fine structure of sub-THz radiation in the experiment with reduced cross-section of the electron beam.

3. Generation of Sub-mm Wave Radiation by a Two-Stage Scheme in a Planar FEM

As the first step of experimental realization of this project we have studied simultaneous generation and transport of two intense relativistic sheet electron beams in two parallel slit channels, which are similar to the electrodynamic system of the proposed two-channel sub-mm wave FEM.

3.1. Experimental setup

In these experiments the parameters of the generated REBs were the following: 0.8 *MeV* electron energy, 3 *kA* total current of each beam, 0.4 *cm* x 7 *cm* cross section and 3 μs pulse duration. The electron beams were applied to drive two parallel channels of the planar FEM with 2D distributed feedback. A schematic of the experimental arrangement is presented in Fig. 9. The interaction circuit of each channel is a planar hybrid Bragg resonator, formed by the upstream 2D and the output 1D Bragg reflectors with a length of 20 *cm* each, connected by a regular waveguide section with a cross section of 0.95 *cm* x 9 *cm* and a length of 32 *cm* in a guiding magnetic field of up to 1.7 *T* [21]. The upstream reflector has a 2D chessboard profile with a period of 4 *mm* and a corrugation depth of 0.17 *mm*, the downstream reflector has a 1D rectangular profile with a corrugation depth of 0.07 *mm*. To eliminate the influence of parasitic modes due to reflection from the side walls of the 2D reflector we used a wave disperser with comb surface which consists of conducting segments inclined at a random angle with a period of 2 *cm* [21]. The undulator has a period of 4 *cm* with 12 *cm* long field tapering sections and a maximum transverse magnetic field of 0.17 *T*.

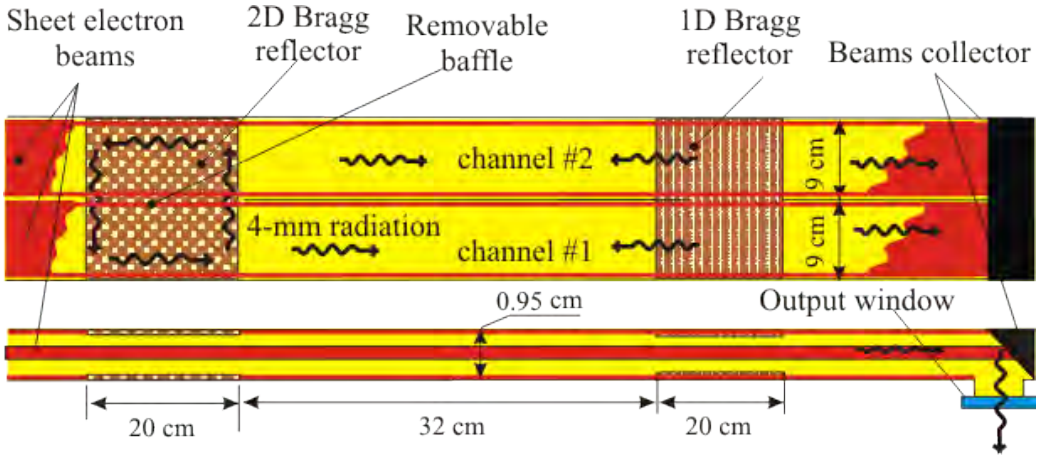

Fig. 9 Scheme of the two planar channel FEM experiment (side view-upper part, plan view-lower part).

In the first series of experiments the two channels of the planar FEM were separated by a baffle in the region of the 2D Bragg reflectors. Nevertheless some inter channel diffraction coupling can take place in the output section. After passing the resonators the REBs are transported to the collectors. Here after beam cross-section expansion using a diverging magnetic field, the beams are dumped in graphite blocks with 45° inclined surface to the beam direction. The mm-wave radiation outgoing from the FEL resonators also passes through these channels to the beam collectors where the wave beams are reflected to the output PTFE (Teflon) windows (thickness $d = \lambda$). From these windows the radiation is transmitted by means of circular waveguides to a specially shielded room for measuring the mm-wave-pulse parameters. The

power of the mm-wave radiation pulse is measured by "hot carriers" detectors in the Ka ($f > 26$ *GHz*) - and W ($f > 70$ *GHz*) - bands. The spectral measurements of the radiation in the W-band at this stage of the experiments were carried out by means of a 4-channel spectral diagnostics including a set of waveguide couplers, band-pass filters and Schottky diodes. The bands of the channels are shown in Fig. 10. The energy of the mm-wave pulse was measured by a Thomas Keating (TK) absolute power/energy meter (1 μJ-0.1 *J*).

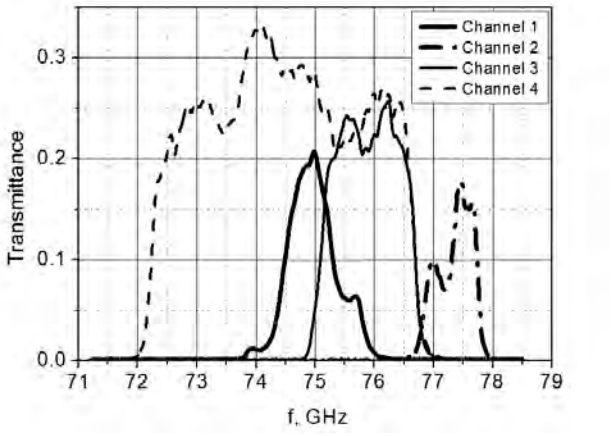

Fig. 10 Transmission bands of the 4-channels spectral diagnostics.

3.2. Experimental results

The results of the first experiments on generation of mm-wave radiation in the two-channel FEM are shown in Fig. 11 which plots the oscilloscope traces of the diode voltage, beam current and mm-wave pulse of a typical shot. Analyzing the data obtained from the 4-channel spectral diagnostics (see Fig. 10) we have observed that in the shots with high values of the mm-wave radiation power, the main power fraction (~70%) is contained in the 1st band (74.5-75.5 *GHz*) and about 30% in the 2nd band (77-77.8 *GHz*). The 3rd channel detects some part of the radiation from the 1st band due to band overlapping. If one subtracts the contribution of the 1st and the 3rd channels from the signal of the 4th channel taking into account the integrals of sensitivity for each channel, the result should be close to zero (see Fig.12). This means that the mm-wave radiation power in the range $72.3 \div 74.5$ *GHz* is rather small in comparison with the power in the 1st and 2nd bands.

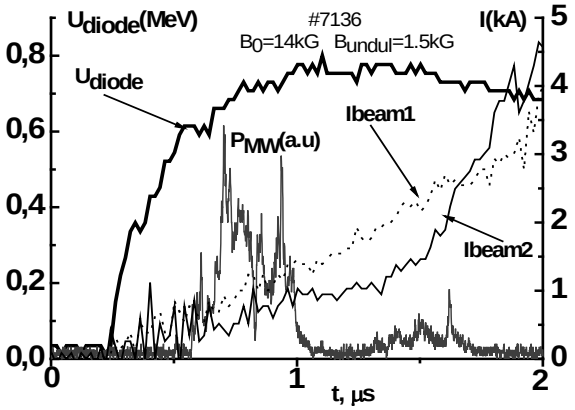

Fig. 11 Traces of a typical FEM shot: U_{diode} is the diode voltage, I_{beam1}, I_{beam2} are the beam currents in two FEM channels, and P_{MW} is the mm-wave radiation power in 1st band of spectral diagnostic.

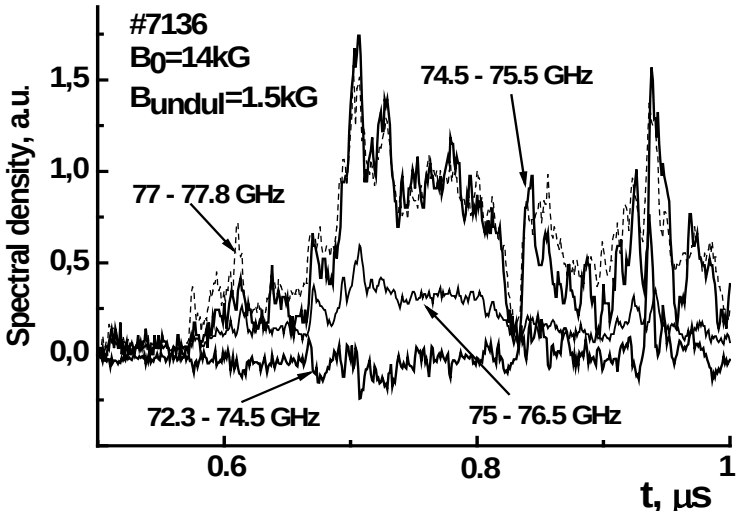

Fig. 12 Spectral densities in the different sub-bands of the W-band 4-channel spectral diagnostics.

As a result the experiments demonstrate that the main part of the generated mm-wave radiation is detected in the 1st frequency band which corresponds to the design frequency and belongs to the longitudinal eigenmodes of our hybrid Bragg resonator [21]. Single-mode operation at the center frequency of 75.1 *GHz* has been experimentally confirmed. The admixture of mm-wave power in the 2nd band is related to parasitic coupling of the TEM and TM_2 waves on the 1D corrugation of the downstream reflector and reflection of the plasma coming from the REB diode.

The next series of measurements have been made to study mm-wave power in these two bands as a function of the undulator magnetic field amplitude at various values of the guide magnetic field. The following Fig. 13 shows this dependence for the 1st and 2nd frequency band, respectively.

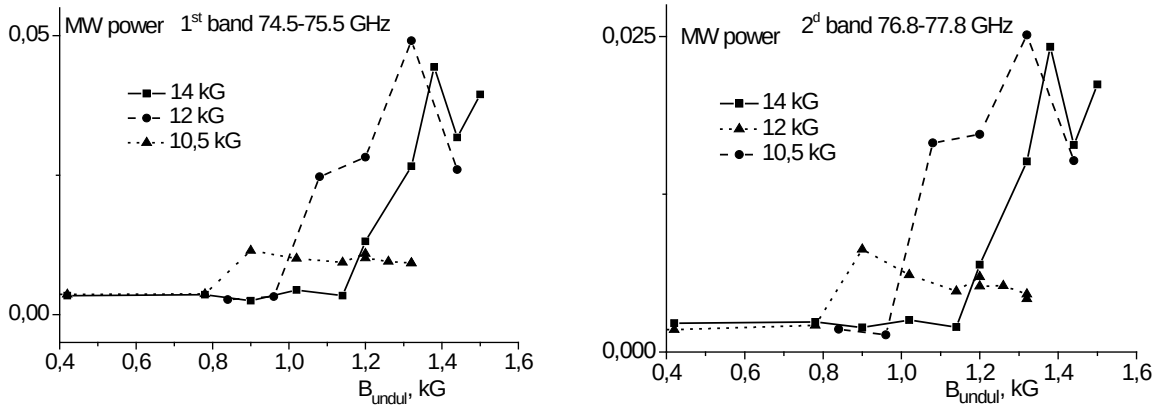

Fig. 13 Dependence of the mm-wave output power in the 1st and 2nd frequency bands on the undulator magnetic field for different guiding magnetic fields.

As can be seen from Fig. 13 the increase of the undulator field above some threshold provides a rapid growth of the mm-wave power from the noise-level to its maximal value, which depends on the guide magnetic field. This behavior agrees well with numerical simulations [22] however

the maximal values measured in the experiments are slightly shifted to higher undulator fields. The direct comparison of theoretical and experimental results is difficult in this case because the start of mm-wave generation occurs at different energies of the beam electrons which are also dependent on the undulator magnetic field. Similar behavior of the radiation power is observed in the 2nd frequency band but at a few times lower power level.

Measurements of the energy of the radiation pulse for frequencies higher than 70 *GHz* by means of the TK absolute power/energy meter gave a value of 4-6 *J* and an average power of 20-40 *MW* from each of the two channels of the FEM.

3.3. Future sub-mm-wave experiments

The principle of generation of sub-mm wave radiation by a two-stage scheme in a planar FEM is the following: the mm-wave radiation generated by the lower sheet REB (see Fig. 9) in a joined planar Bragg resonator of the FEM is scattered on the upper REB with Doppler conversion of the wavelength λ from 4 *mm* (75 *GHz*) to approximately 0.5 *mm* (0.6 *THz*) [10]. First experiments on this two-stage scheme will be carried out in the SASE regime (self-amplification of spontaneous emission). Later experiments will employ advanced tunable Bragg reflectors based on coupling of propagating and cutoff waves. On the basis of such feedback it is possible to combine the mechanisms of mode selection used in gyrotrons and orotrons with Doppler frequency up-conversion. Coupled-wave analysis together with 3D EM simulations show that such advanced Bragg structures are able to provide selectivity up to transverse sizes of 10-20 λ [23]. Compatibility with transportation of an intense REB encourages the use of these novel Bragg reflectors in our sub-mm wave experiment. Tunability can be achieved by variation of the distance between the reflector plates. For a frequency of 0.6 *THz* the period of corrugation is 0.5 *mm* and the corrugation depth e.g. 0.05 *mm*.

4. Development of Novel Quasi-Optical Components and Systems for Sub-mm Wave Diagnostics

A successful realization of sub-THz experiments demands adequate quasi-optical selective components and systems intended for controlling or measuring properties of the radiation beams. As a rule, the best solution is attained when such components are implemented on basis of planar regularly patterned metallized microstructures of sub-wavelength topology. Appropriate choice of topology enables to control amplitude, phase and polarization response of the structure and allows easy fabrication via well-proven photolithographic or other micromachining techniques of micrometer accuracy [24-26]. Commonly referred to in the literature as frequency selective surfaces (FSSs) [27], such structures are resonant-kind and are exploited under conditions when the resonance frequency $\omega_{res}=2\pi c/\lambda_{res}$ lies below the point of the diffraction lobes onset: $g/\lambda_{res}<1/[1+\sin\theta]$ (here g, λ_{res}, θ, c are the FSS lattice constant, operating wavelength, radiation incidence angle, and light speed respectively). For filter applications, FSSs with a moderate-scaled topological micro-pattern ($g\sim0.3\div0.7\ \lambda_{res}$) are typically utilized, while more sub-wavelength FSSs ($g<<\lambda_{res}$) are used as the basic elements in planar EM metamaterials [28].

In our R&D activities, we elaborated a broad line of passive FSS-based quasi-optical components designed for operation frequencies from 0.05 *THz* up to several THz [25-26]. The

components include frequency filters, beam splitters, polarization and phase transformers, focusing devices, and thin resonant absorbers, which are produced in a qualified cycle of the consecutive stages: Full-wave electromagnetic analysis → Lithographic fabrication → Spectral characterization [25]. In this paper we present recent results on developing band-pass FSS-filters for plasma diagnostics and ultra-thin metamaterial absorbers for sub-THz imaging.

4.1. THz bandpass filters using frequency selective surfaces

In [29] we developed an original 4-channel radiometric system intended for spectral measurements of sub-THz emission in the GOL-3 plasma experiments in four parallel frequency-shifted spectral bands overlapping the range 250-420 *GHz*. The system was built on a scheme with quasi-optical de-multiplexing of the input radiation beam onto four spatially separated channels with subsequent frequency filtering by quasi-optical FSS-filters and spectral signal detection by Schottky detectors matched with receiving horn-lens antennas (Fig. 14). The FSS-filters were implemented as bi-layer interference structures embedded into polypropylene (PP) with the following configuration: "320μmPP+FSS+160μmPP+FSS+320μmPP", where "320μmPP" and "160μmPP" designate PP-films with the specified thickness. The topology of inductive anisotropic resonant dipole slots (Fig. 14a) was utilized for the FSSs, which were produced by photolithographic pattering of the aluminum layer (0.4 μm thick) deposited on the surface of bearing PP-films, as described in [25], and further fused into the interference structure via a hot lamination technique. Anisotropic topology was chosen to realize ~35-38 *GHz* frequency shift of the transmission bands for orthogonally polarized radiation components. This allowed us to employ only two hardware filters for implementing 4 spectral channels in order to reduce the total fabrication costs. These FSS-filters demonstrated a transmission bandwidth of ~40 *GHz* at an out-of-band attenuation -20 to -30 *dB* with maximum transmission of ~50%.

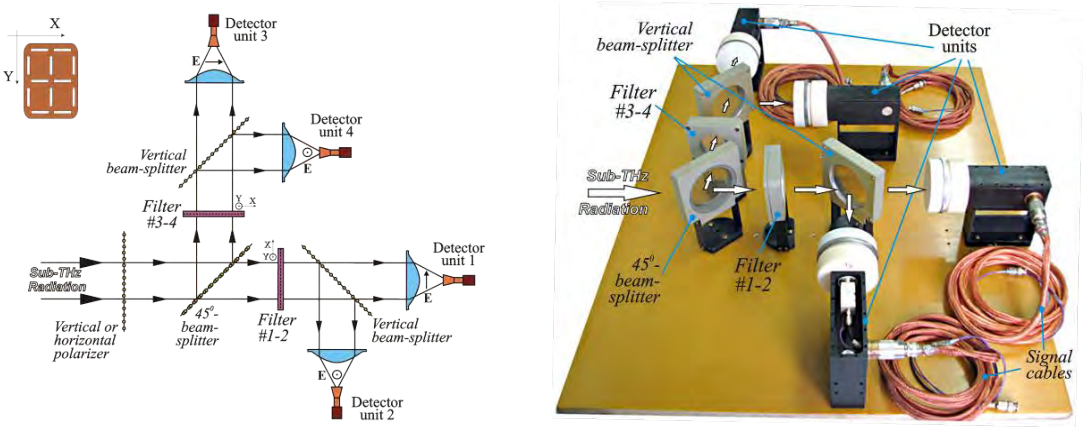

(a) (b)

Fig. 14 Principal experimental set-up (a) and photograph (b) of the 4-channel radiometric system (250-420 *GHz*) for GOL-3 plasma experiments.

For next year's GOL-3 experiments, the 4-channel radiometric system was recently upgraded to an 8-channel one. This 8-channel system overlaps the frequency band ~100-400 *GHz* and is intended for spectral measurements of sub-THz emission both in the vicinity of the second and the first harmonics of the plasma frequency. For the upgraded system we developed a new set of the band-pass high-performance FSS-filters with improved selectivity, which include 8 polarization insensitive structures based on isotropic FSSs. Our experience showed that isotropic

FSSs proved to be more convenient for multi-channel systems due to the opportunity of independent adjustment of all spectral channels when changing the filters.

Unlike the aforementioned filters from the 4-channel system, each of the new filters are comprised by three substrate-free self-bearing copper FSSs 8 μm thick, which differ in lattice constants and are designed as multiplex (non-interference) structures. The new FSSs have the topology of hexagonally-packed inductive tripole slots (Fig. 15) and were fabricated by an electroplating technique, which was specially adapted in this work to the THz filter implementation.

The stages of FSS fabrication by the electroplating technology are illustrated in Fig. 15. The process starts with chemical treatment and polishing of the metallic wafer with outer dimensions 100 mm × 100 mm (*1*) followed by spin coating of a 10 μm thick positive photo-resist film, which is then air dried and thermally treated in a thermostat at 90 ℃ (2). After putting the photo-resistive layer into a hard contact with a FSS photo-mask represented by a quartz wafer with a patterned ferric-oxide-film (*3*), the photo-resist is exposed to monochromatic UV-radiation (λ = 365 nm) through the photo-mask (*4*) to create a latent FSS image, which topological micro-pattern replicates the FSS micro-pattern on the photo-mask. The latent image is further chemically developed in alkaline solution, which removes the irradiated (transparent) areas of the photo-resist (*5*). Subsequent hardening of the developed photo-resist by drying and thermal treatment at 120 ℃ (*6*) forms the firm resistive mask, through which the 8 μm thick copper layer is further electroplated on the conducting wafer from a copper-bearing bath (*7*). After removing the hardened resistive mask by dissolving in an organic solvent (*8*), the grown FSS is detached from the wafer (*9*) and fixed on a ring-shaped metal holder inside the FSS-filter shell at typical clear aperture diameter 50-70 mm (*10*).

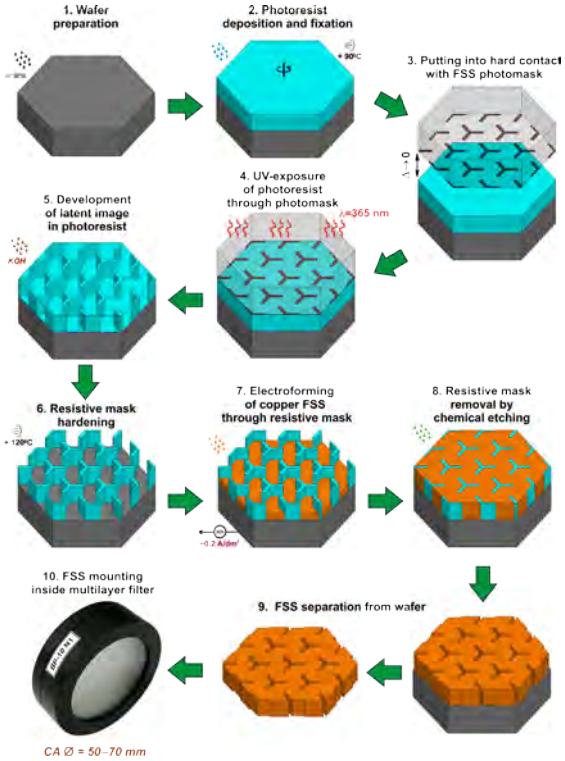

Fig. 15 Stages for producing substrate-free copper FSS by the electroplating technology.

The spectral responses of the eight developed quasi-optical filters based on electroplated FSSs are shown in Fig. 16. The filters were designed to have the central frequencies ν_{max} of the transmission bands in GHz as follows: 112, 132, 156, 188, 224, 264, 312, and 376. Compared to the PP-based interference filters, the electroplated multiplex filters exhibited a much better performance, having a transmission maximum of $> 90\%$, a relative bandwidth (FWHM) of ~12%, and an out-of-band transmission at the higher frequency edge of $<10^{-4}$. Note that at the low frequency edge ($\nu < \nu_{max}$) the filter transmission exhibits a quasi-exponential frequency response, while at high frequencies the transmittance is stabilized on the level of a quasi-plateau. The filters were characterized in the frequency range 100-1100 *GHz* under atmospheric conditions by using a backward wave oscillator (BWO) spectroscopy technique with frequency multiplication [25]. The photograph of the experimental set-up for transmission measurements is presented in Fig.17. Due to instrumental restrictions, a set of BWOs was employed to overlap only the frequency band 0.10-0.38 *THz*. With the Golay-cell THz detector and lock-in amplifier used for measuring a 23 *Hz* chopper-modulated BWO beam, the instrumental level of the minimal transmission detectability (inversed dynamic range) for this band was estimated as $3 \cdot 10^{-7}$ on average (Fig. 17) due to high values of the output radiation power (~2-20 *mW*) for the utilized BWOs.

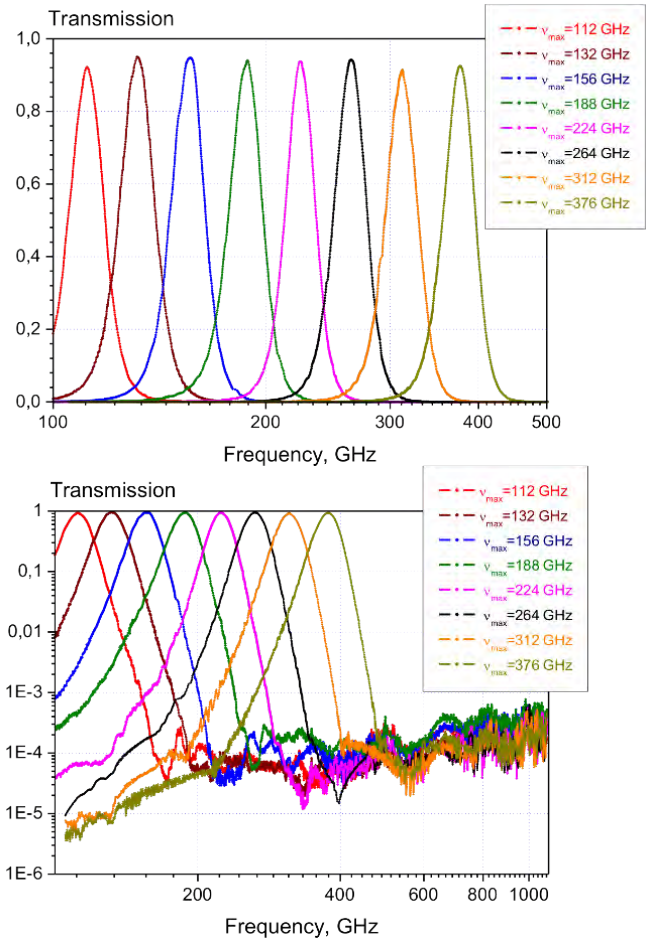

Fig. 16 Frequency response in linear *(top)* and logarithmic *(bottom)* scales for eight developed 3-layered multiplex FSS-filters measured with a quasi-optical BWO-spectrometer. Characterization was performed at normal incidence.

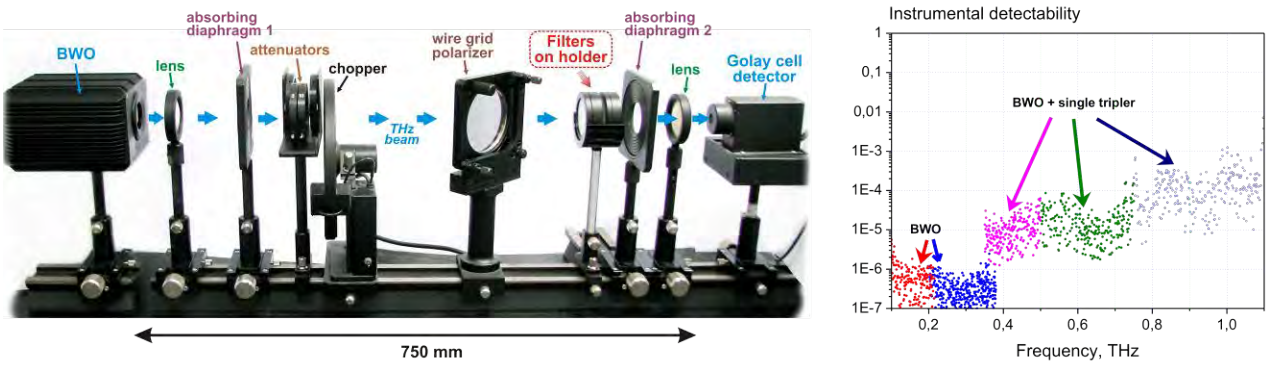

(a) (b)

Fig. 17 Quasi-optical set-up used for measuring transmission of the band-pass filters *(a)* and spectral behavior of the instrumental detectability *(b)*.

The instrumental detectability was determined as the transmission signal when the absorbing diaphragm 2 was substituted by a fully opaque absorbing screen with diffusively scattering surfaces. To characterize filters in the frequency range 0.38-1.10 *THz*, we exploited BWOs combined with VDI™ frequency triplers. The unavoidable power losses due to frequency conversion, partially enhanced by atmospheric attenuation, led to a degradation of the instrumental detectability threshold up to $5 \cdot 10^{-6}$-$2 \cdot 10^{-4}$ (Fig. 17).

4.2. Real-time terahertz imaging using metamaterial absorbers

The key drawback of commonly used THz sensors based on semiconductor and superconductor structures is related with the high complexity of their on-chip micro/nano-element integration & micro/nano-machining fabrication, unsuitable for large-format array mass production, or with the necessity of a cryogenic environment. Similarly, the attempts for direct adaptation of modern room-temperature IR bolometric and pyro-electric array cameras, as well as fluorescence- quenching-based thermal image plates to THz imaging typically reveal either the problems of faint susceptibility or dimension restrictions for the radiation sensitive area, poorly applicable for handling radiation beams with diameters above 20 *mm*. Due to the aforementioned limitations, high-quality THz imaging is typically realized via a time-consuming procedure of 2D raster scanning in a scheme with single detector measurements.

A very prospective approach for bolometric detection of THz radiation employs the principle of THz-to-IR conversion [26]. Such converters are flexible in the choice of the operating wavelength and have no principle constraint on the array's overall dimensions. It is essential that adaptation of these detectors to the sub-mm-wave band became feasible due to elaboration of the concept of electrically thin electromagnetic absorbers with a close to unity absorption within a desired frequency range [30-32]. Such absorbers are considered as a kind of metamaterial structures and are typically implemented in a configuration of a high-impedance or artificial impedance surface (HIS or AIS), which is represented by a sub-wavelength frequency-selective surface (FSS) of a capacitive type placed over a thin metal-backed dielectric substrate [30], [33]. Unlike the classical electromagnetic absorbers based on unfavorably thick quarter-wave absorbing layers [34], the AIS-absorbers have a very large ratio of free-space wavelength λ to absorber thickness d. The condition $\lambda / d >> 1$ is essential for decreasing the absorber's heat capacity which allows achieving high sensitivity and low response time of the bolometric

detector. It is noteworthy that the increase of the ratio λ / d inevitably leads to smaller absorption bandwidth, making AIS-absorbers ideally suitable for bolometric detectors with high spectral resolution.

In this paper we present the results of experimental development of spectrally selective high-performance AIS-based absorbers with wavelength-to-thickness ratios $\lambda / d \cong 40\text{-}50$ designed for bolometric applications at frequencies 0.3-0.4 *THz*. To maximize the absorption resonance Q-factor, as well as the ratio λ / d, the absorbers are implemented on the basis of low-loss bulk materials, such as polypropylene (PP) dielectric films and high-conductivity aluminum metallization, that distinguishes them from any types of absorbers realized before. The concept of a THz-to-IR converter with integrated AIS-absorbers has been developed, and the efficiency of this approach is demonstrated in "THz-to-IR conversion" experiments on imaging sub-mm-wave beams from a backward wave oscillator (BWO) with mW output radiation power level.

4.2.1. Experimental results

The Figs.18 and 19 show ultra-thin polarization-selective AIS-absorbers designed for the frequency range 0.30-0.36 *THz*. The photolithographically-patterned split-ring resonator arrays (SRR), optimized using the Ansoft HFSS™ software, were utilized as via-free FSSs to realize the AISs of the "FSS + grounded dielectric slab" configuration. Polypropylene (PP) with a thickness of d = 20 μm was used as the AIS dielectric substrate, which was metalized from both sides via thermal vacuum deposition of 0.4 μm thick aluminum to form the high-conductivity metallization of the "grounded" and FSS layers.

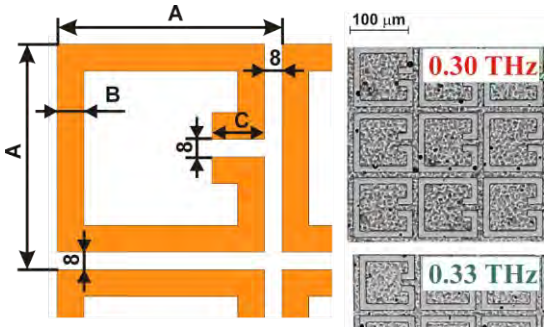

THz	A	B	C
0.30	110	12	27.5
0.33	102.8	12.2	24
0.36	100.5	14.3	14.9

Fig. 18 Micrographs and geometries of the topological patterns for SRR FSSs fabricated on PP surface for the 0.3 *THz*-, 0.33 *THz*-, and 0.36 *THz* absorbers. All dimensions are in μm.

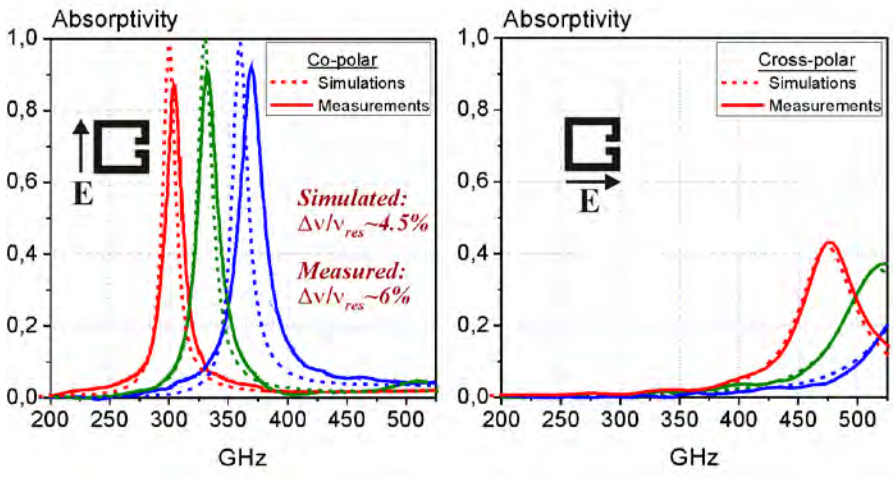

Fig. 19 Spectral response of the three different PP-based absorbers (d = 20μm) optimized for near-unity co-polar absorbance at 0.30 *THz*, 0.33 THz and 0.36 *THz* (λ/d ratios are 50, 45 and 41 respectively).

The developed AIS-absorbers were used to design a simple and flexible bolometric system for active THz imaging employing the scheme of THz-to-IR conversion [26]. Here the THz beam is visualized via detecting THz-induced thermal heating of the absorber by a conventional infrared camera (see Figs. 20 and 21). It is noteworthy that the proposed imaging system operates in real time and suits well for imaging THz beams at mW CW power or higher, though the negative effects of the "comet tail" and blooming can be identified on the registered images (see Fig. 21). These effects can be reduced via employing AIS-absorbers with a thinner dielectric substrate and an appropriately redesigned FSS pattern.

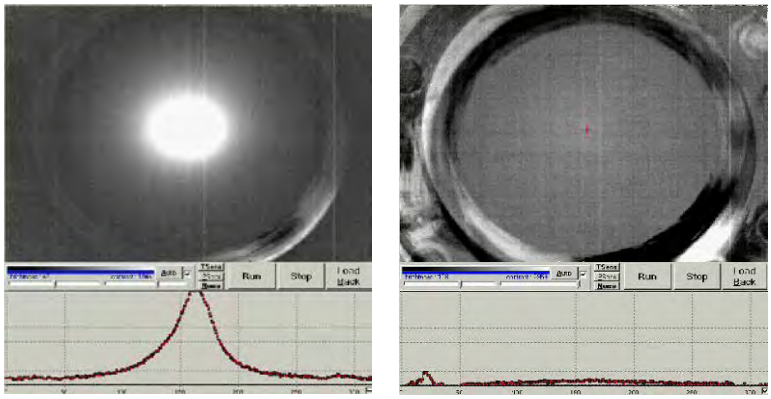

(a) (b)

Fig. 20 IR images of a 3 *mW* BWO beam focused upon the "0.3 *THz* absorber" with clear aperture diameter of 32 *mm*: (a) co-polar excitation (E ⊥ SRR gaps, 0.3 *THz*); (b) cross-polar excitation (E || SRR gaps, 0.3 *THz*). The bottom graphs indicate the intensity distribution along the horizontal line traced through the red crosshair.

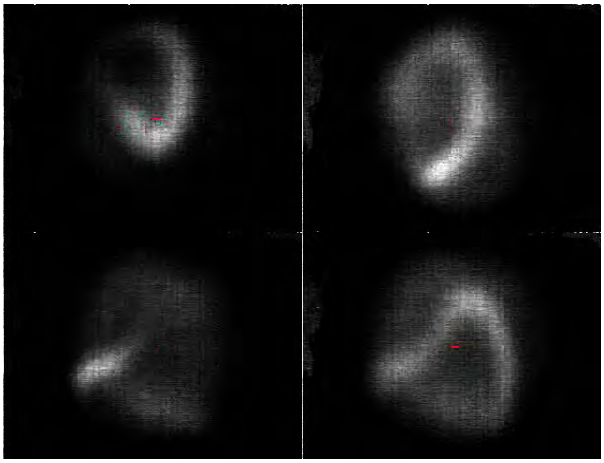

Fig. 21 Screen shots from a recorded real-time THz imaging movie: Motions of the focused BWO sub-mm-wave beam.

Acknowledgements

Herewith we gratefully acknowledge the support of this research by the Russian Federation Government Grants No. 11.G34.31.0033 and NSh 7792.2010.2, by the Contract #16.740.11.03.77 of the Ministry Education and Science of the Russian Federation, by the contract 16.740.11.0377 of the Federal Target Program, and by the Program 30 of Russian Academy of Sciences. We also acknowledge A.V. Gelfand, Dr. M. A. Dem'yanenko and M.A. Astafyev for technological support in manufacturing FSS structures and in THz measurements.

References

[1] R.E. Aamodt, W.E. Drummond, "Non-linear Coupling of Plasma Oscillations to Transverse Waves", *J. Nucl. Energy, Part C*., 6, 147-152, (1964).

[2] V. N. Tsytovich, "Theory of Turbulent Plasma", *New York: Consultants Bureau*, (1977).

[3] E.N. Kruchina, R.Z. Sagdeev and V.D. Shapiro, "Strong Langmuir Turbulence as a Source of Radio Emission", *JETP Lett.*, 32, 419-423, (1980).

[4] S.A. Colgate, E.P. Lee, M.N. Rosenbluth, "Radio Emission from a Turbulent Plasma", *Astrophysical J.*, 162, 649-664, (1970).

[5] V. V. Zheleznyakov, "Electromagnetic Waves in Cosmic Plasma. Generation and Propagation", *Moscow: Nauka*, (1977).

[6] B.N. Breizman, D.D. Ryutov, "Powerful Relativistic Electron Beams in a Plasma and in a Vacuum (Theory)", *Nuclear Fusion*, 14, 873-907, (1974).

[7] A.V. Arzhannikov, S.A. Kuznetsov, A.V. Burdakov et al., "Subterahertz Emission at Strong REB-Plasma Interaction in Multimirror Trap GOL-3", Fusion Science and Technology, 59,74-77, (2011).

[8] A.V. Arzhannikov, A.V. Burdakov, P.V. Kalinin, et al. "Subterahertz Generation by Strong Langmuir Turbulence at Two-Stream Instability of High-Current 1-MeV REBs", *NSU Bulletin, Series: Physics,* 2010, 5, 4, 44-49, (2010).

[9] A.V. Arzhannikov, N.S. Ginzburg, P.V. Kalinin, et al. "Investigation of Mode Structure for mm-Wave Radiation Pulses Generated by Planar FEM at 2-D Distributed Feedback", *Proc. 16th Int. Conf. on High-Power Particle BEAMS, BEAMS'2006*, Oxford, UK, 1, 208-213, (2006).

[10] A.V. Arzhannikov, N.S. Ginzburg, et al., "Intercavity Scattering Scheme for Two-Stage Generation of Submillimeter Radiation on the Base of Planar 2D Bragg FEM", *Proc. Int. Workshop "Strong Microwaves in Plasma", Nizhny Novgorod, Russia*, 1, 228-232, (2006).

[11] S.L. Sinitsky, A.V. Arzhannikov, V.T. Astrelin, et al., "Simultaneous Generation and Transport of Two Microsecond Sheet REBs in Application to Multichannel FEM", *IEEE Transactions on Plasma Science*, 37, 1885-1889, (2009).

[12] A. Burdakov, A. Arzhannikov, V. Astrelin, et al., "Plasma Heating and Confinement in GOL-3 Multimirror Trap", *Fusion Science and Technology*, 51 (2T), 106-111, (2007).

[13] A. Burdakov, A. Arzhannikov, V. Astrelin, et al., "Status and Prospects of GOL-3 Multiple Mirror Trap", *Fusion Science and Technology*, 55 (2T), 63-70, (2009).

[14] V.V. Postupaev, A.V. Arzhannikov, V.T. Astrelin, et al., "Experiments with "Thin" Electron Beam at GOL-3" *Fusion Science and Technology*, 59 (1T), 144-149, (2011).

[15] V.T. Astrelin, A.V. Burdakov, V.V. Postupaev, "Generation of Ion-Acoustic Waves and Suppression of Heat Transport during Plasma Heating by an Electron Beam", *Plasma Phys. Reports*, 24, 414-425, (1998).

[16] A.V. Arzhannikov, V.T. Astrelin, A.V. Burdakov, et al., "Direct Observation of Anomalously Low Longitudinal Electron Heat Conductivity in the Course of Collective Relaxation of High-Current Relativistic Electron Beam in Plasma". *JETP Lett.*, 77, 358-361, (2003).

[17] A.V. Arzhannikov, V.T. Astrelin, A.V. Burdakov, et al., "Study of the Mechanism for Fast Ion Heating in the GOL-3 Multimirror Magnetic Confinement System", *Plasma Phys. Reports*, 31, 462-475, (2005).

[18] A.D. Beklemishev, "Bounce Instability in a Multi-Mirror Trap", *Fusion Science and Technology*, 51 (2T), 180-182, (2007).

[19] V.V. Postupaev, A.V. Arzhannikov, V.T. Astrelin, et al., "Role of q-Profile for Plasma Confinement in the Multimirror trap GOL-3", *Fusion Science and Technology*, 47 (1T), 84-91, (2005).

[20] V. V. Tirsky, V.G. Ledenev and V.M. Tomozov, "Concerning the Electromagnetic Radiation Spectrum of a Hot Plasma with Langmuir Turbulence in a Magnetic Field", *Physica Scripta*, 64, 353-359, (2001).

[21] A.V. Arzhannikov, N.S. Ginzburg et al., "Generation of Spatially Coherent Radiation in Free Electron Masers with Two Dimensional Distributed Feedback", *JETP Lett.*, 87, 618 – 622, (2008).

[22] N.V. Agarin, A.V. Arzhannikov, V.B. Bobylev, et al., "Operation of High-Power Planar FEM with Two-Dimansional Bragg Reflectors", *Proc. 13th Int. Conf. on High-Power Particle Beams*, Nagaoka, Japan, 1, 244-247, (2001).

[23] P.V. Kalinin, A.V. Arzhannikov, S.A. Kuznetsov, et al., "Short-Wavelength Tunable Bragg Reflectors based on Coupling of Propagating and Cutoff Waves: Modeling and Cold Tests", *Proc. 8th Int. Workshop "Strong Microwaves and Terahertz Waves: Sources and Applications"*, Nizhny Novgorod, Russia, 86-87, (2011).

[24] P.A.R. Ade et al.,"A Review of Metal Mesh Filters", *Proc. SPIE*,6275, 62750U-1–62750U-15, (2006).

[25] S.A. Kuznetsov, A.V. Arzhannikov, V.V. Kubarev, et al., "Development and Characterization of Quasi-Optical Mesh Filters and Metastructures for Subterahertz and Terahertz Applications", Key Engineering Materials, 437, 276-280, (2010).

[26] S.A. Kuznetsov, A.G. Paulish, A.V. Gelfand, et al. "Bolometric THz-to-IR Converter for Terahertz Imaging", *Appl. Phys. Lett.*, 99, 023501 1-3 (2011).

[27] B. Munk, "Frequency Selective Surfaces: Theory and Design", *NY: Wiley*, (2000).

[28] N. Engheta, R.W. Ziolkowski,"Electromagnetic Metamaterials: Physics and Engineering Explorations", *Wiley and IEEE Press*, (2006).

[29] S.A. Kuznetsov, A.V. Arzhannikov, Yu.G. Goncharov, et al., "Quasi-Optical Spectral System for Submm-Wave Radiometry of Turbulent Plasma", *Proc. 39th European Microwave Conference (EuMC-2009)*, Rome, Italy, 173-176, (2009).

[30] O. Luukkonen, F. Costa, C.R. Simovski, et al. "A Thin Electromagnetic Absorber for Wide Incidence Angles and Both Polarizations", *IEEE Trans. on Antennas and Propagation*, 57, 3119–3125 (2009).

[31] H. Tao, A.C. Strikwerda, K. Fan, et al. "Highly Flexible Wide Angle of Incidence Terahertz Metamaterial Absorber: Design, Fabrication, and Characterization", *Phys. Rev. B.*, 78, 241103-1-4 (2008).

[32] X. Liu, T. Starr, A.F. Starr, et al. "Infrared Spatial and Frequency Selective Metamaterial with Near-Unity Absorbance", *Phys. Rev. Lett.*,104, 207403-1–4 (2010).

[33] C.A. Balanis, "Modern Antenna Handbook", *Wiley-Interscience*, (2008).

[34] K.J. Vinoy, R.M. Jha R., "Radar Absorbing Materials: From Theory to Design and Characterization", *Kluwer Academic Publishers*, (1996).